Monte Carlo Simulation of Electron Transport in Quantum Cascade Lasers

Oskar Baumgartner, Zlatan Stanojević, and Hans Kosina

Abstract. A transport model for quantum cascade lasers based on the Pauli master equation is presented. An efficient Monte Carlo solver has been developed. The numerical methods to reduce the computational cost are discussed in detail. Finally, the simulator is used to obtain current-voltage characteristics as well as microscopic quantities of a mid-infrared QCL structure.

Keywords. Pauli Master Equation, Quantum Cascade Lasers, Electron Transport.

Mathematics Subject Classification 2010. 90C15, 90C30, 90C59, 62L20.

7.1 Introduction

Quantum cascade lasers (QCLs) offer a wide range of advantages which make them a popular choice for coherent light sources [5]. Their light emission is based on intersubband transitions. Due to the periodic nature of QCLs, a single electron will repeatedly contribute to the photon emission. The properties of the laser are mainly determined by the designer's choice of material and quantum well geometry.

For this purpose, simulation is a useful tool for tuning the QCL design to the desired optical and electrical characteristics. A requirement for such a simulator as design tool is a good balance between computational speed and physical accuracy. To describe the electronic properties of the laser, a quantum mechanical transport model is necessary. Previously the nonequilibrium Green's function formalism (NEGF) has been used as a rigorous approach to capture the QCL's physics [10, 11]. Unfortunately the inherently high computational costs of the NEGF formalism render it unfeasible as a design tool.

7.2 QCL Transport Model

In our approach we use the Pauli master equation (PME) [4] to model current transport through the QCL's semiconductor heterostructure. Based on the experiences of a MATLAB prototype presented in [14], an optimized Monte Carlo (MC) simulator has

been implemented in C++ within the Vienna–Schrödinger–Poisson (VSP) simulation framework [9].

7.2.1 Pauli Master Equation

Theoretical studies showed that in many practical cases the steady state transport in QCLs is incoherent such that a semiclassical description can be employed [7, 8]. Following this approach, we developed a transport simulator for quantum cascade lasers based on the Pauli master equation [14]. The transport is described via scattering transitions among quasistationary basis states which are determined by numerically solving the Schrödinger equation. The Hamiltonian includes the band edge formed by the heterostructure. In this way, tunneling is accounted for through the delocalized eigenstates.

The transport equations are derived from the Liouville–von Neumann equation in the Markov limit in combination with the diagonal approximation. This means that the off-diagonal elements of the density matrix are neglected and one arrives at the Boltzmann-like Pauli master equation [6]

$$\frac{\mathrm{d}\, f_{\mathbf{k},n}(t)}{\mathrm{d}t} = \sum_{\mathbf{k}',m} \left\{ S_m^n \left(\mathbf{k}', \mathbf{k}\right) f_{\mathbf{k}',m}\left(t\right) - S_n^m \left(\mathbf{k}, \mathbf{k}'\right) f_{\mathbf{k},n}\left(t\right) \right\}.$$

Here, m and n denote the subband indices, and $\mathbf{k}$ and $\mathbf{k}'$ the in-plane wave vectors. The transition rate from state $|\mathbf{k}', m\rangle$ to state $|\mathbf{k}, n\rangle$ for an interaction H_{int} follows from Fermi's golden rule

$$S_n^m \left(\mathbf{k}, \mathbf{k}'\right) = \frac{2\pi}{\hbar} \left| \langle \mathbf{k}', m | H_{\mathrm{int}} | \mathbf{k}, n \rangle \right|^2 \delta \left(\mathcal{E}(\mathbf{k}') - \mathcal{E}(\mathbf{k}) \mp \hbar\omega \right).$$

We make use of the translational invariancy of the QCL structure and simulate the electron transport over a single stage only. The wave function overlap between the central stage and spatially remote stages is small. It is therefore assumed that interstage scattering is limited only to the nearest neighbor stages and that interactions between basis states of remote stages can be safely neglected.

The states of the whole QCL device structure are assumed to be a periodic repetition of the states of a central stage. This approach ensures charge conservation and allows imposing periodic boundary conditions on the Pauli master equation.

Since transport is simulated over a central stage only, every time a carrier undergoes an interstage scattering process the electron is reinjected into the central stage with an energy changed by the voltage drop over a single period. The total current is determined by the net number of interstage transitions.

The transport equations can be solved using a Monte Carlo approach. We developed an algorithm and devised several new numerical methods to reduce the computational cost of the simulation. The implementation details will be discussed in Section 7.2.3.

7.2.2 Calculation of Basis States

The task at hand can be divided into two parts. First, the basis states need to be determined. Second, the states have to be assigned to a stage according to their periodicity. For this purpose the equation definition and solver facilities of the VSP were used beneficially.

Since it is essential to consider band nonparabolicity for QCLs, the user can choose one of several models for the Hamiltonian of the Schrödinger equation. For this purpose, in addition to the single band effective mass model, an effective two-band $\mathbf{k}\cdot\mathbf{p}$ model [16] or a three-band $\mathbf{k}\cdot\mathbf{p}$ model are available.

To describe the openness of the quantum system we make use of the perfectly matched layer (PML) boundary conditions for the Schrödinger equation [15]. Perfectly matched layers were originally used as boundary conditions for electromagnetic and waveguide problems [1]. The PML boundary conditions give rise to a complex eigenvalue problem. It is solved by means of Arnoldi iteration and the ARPACK [12] library linked to VSP. The calculated eigenvectors correspond to the complex wavefunctions. The real part of the eigenvalue is the eigenenergy of the quasibound state, whereas the imaginary part is related to its finite lifetime due to the openness of the system. This allows us to estimate the tunneling current using the following relation [2]:

$$J_{\text{Tunnel}} = \sum_i \frac{n_i}{\tau_i}.$$

As long as the hereby calculated tunneling current is small compared to the incoherent current, the semiclassical approach of the PME remains valid.

We calculated the eigenstates for an $In_{0.53}Ga_{0.47}As$ / $GaAs_{0.51}Sb_{0.49}$ mid infrared (MIR) quantum cascade laser reported in [3]. The barrier thicknesses (in bold) and the well thicknesses of one period in nanometer are **7.5**/2.9/**1.5**/6.5/ **1.8**/5.9/**5.5**/5.6/**2.6**/5.1/**2.0**/5.2/**4.0**/4.2/**2.9**/4.4. The underlined layer is doped to a concentration of $4 \times 10^{17}\text{cm}^{-3}$. We will use this device as a benchmark throughout this chapter. The calculated wavefunctions for a two-band $\mathbf{k}\cdot\mathbf{p}$ Hamiltonian with PML boundary conditions are shown in Figure 7.1.

To use the eigenvectors as basis states in the MC routine we need to consider the periodicity of the device and automatically select the field-periodic states of a single stage. For that purpose we calculate the crosscorrelation and autocorrelation $C_{ij}(x) = \Psi_i(x) \star \Psi_j(x)$ of all subbands. We make use of the relation $\mathcal{F}\{\Psi_i \star \Psi_j\} = \mathcal{F}\{\Psi_i\}^* \cdot \mathcal{F}\{\Psi_j\}$ and the Fast Fourier Transform to quickly obtain the correlations, i. e., $C_{ij}(x) = \mathcal{F}^{-1}\{\mathcal{F}\{\Psi_i\}^* \cdot \mathcal{F}\{\Psi_j\}\}$. Then the positions $x_{ij,\max}$ of the maxima of the correlations $C_{ij}(x)$ are determined for all the subbands. If $x_{ij,\max}$ lies at the geometric period length L of the QCL structure, the two states i and j are considered field-periodic and given an appropriate stage index. As an example the field-periodic states of the InGaAs/GaAsSb QCL are given in Figure 7.2.

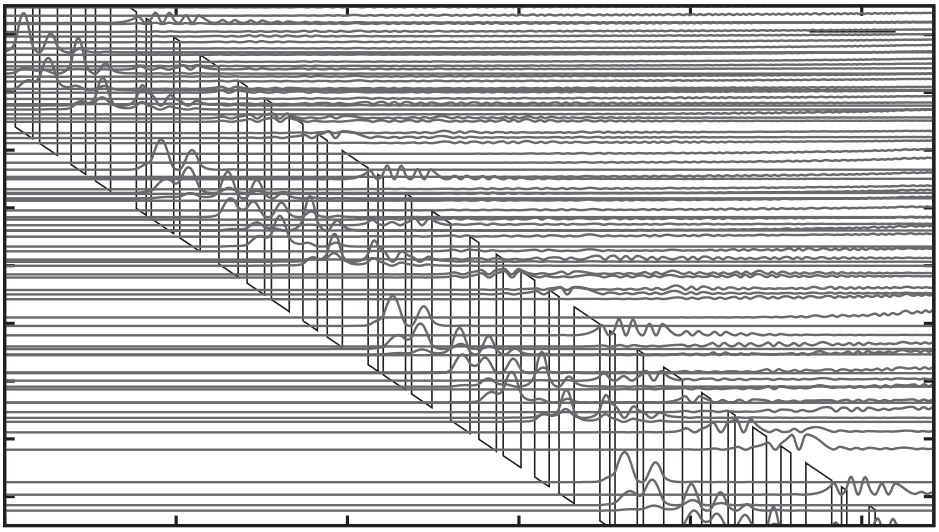

Figure 7.1. Multiple cascades of a QCL need to be considered om order to obtain suitable basis states for the PME Monte Carlo solver.

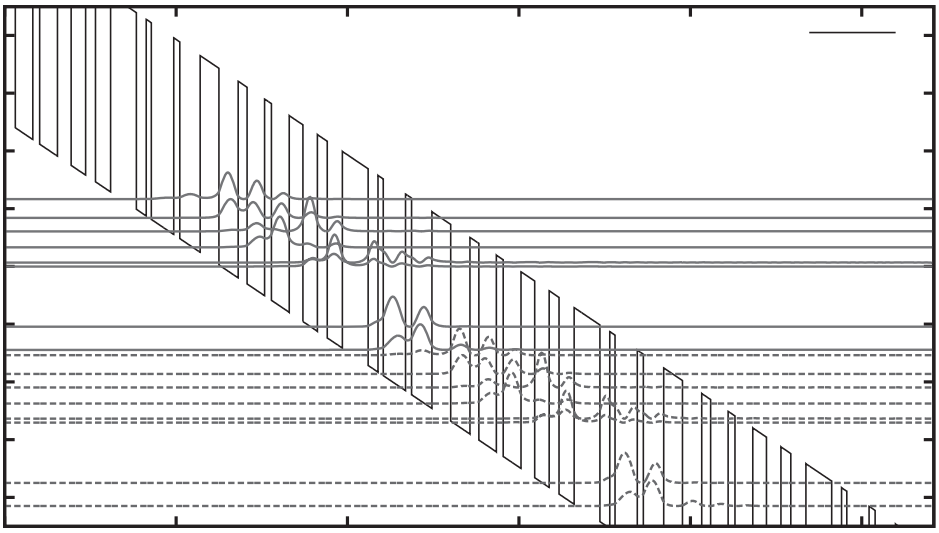

Figure 7.2. Application of our subband selection routine which automatically assigns the field-periodic wavefunctions to a stage of the QCL (only the states of two stages are shown).

7.2.3 Monte Carlo Solver

The wavefunctions provided by the routines discussed above are processed to initialize the MC code. After calculating the scattering rates using functor classes and filling the data structures, the initial valley, subband, and energy of the carrier are randomly selected. In the MC loop the precalculated possible scattering processes are looked up for the actual electron state. A random number r is determined using a uniform distribution in the interval $[0, P_n]$ where $P_n = \sum_{j=1}^{n} \Gamma_j$ is the total scattering rate. The scattering process i is selected from the table such that the relation $P_{i-1} < r \leq P_i$

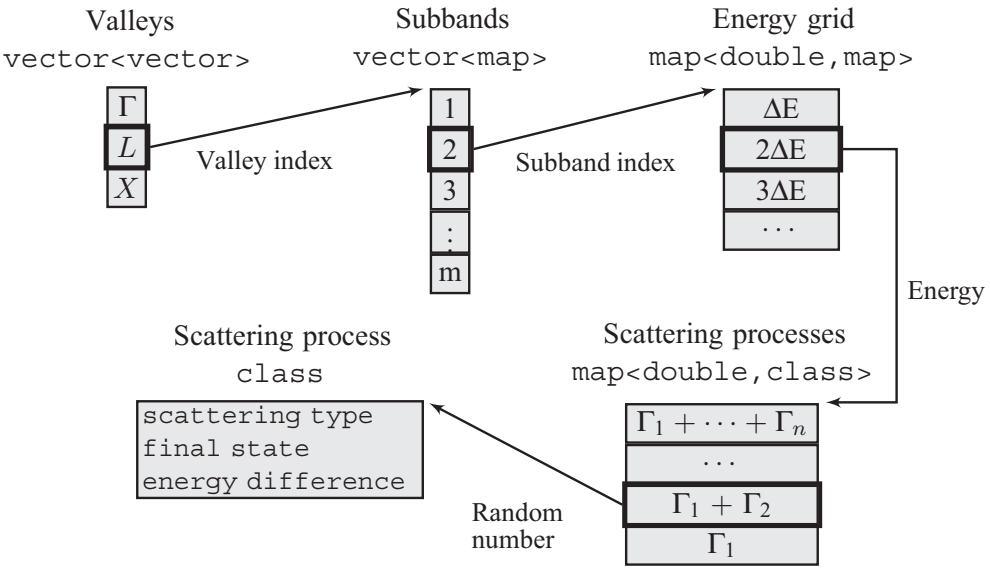

Figure 7.3. Data structures for the selection of a scattering process. Valleys and subbands are accessed by index. Each subband uses its own energy grid. For a fast lookup the grid is implemented as a C++ standard template library (STL) `map` with the energy as key value. Similarly, scattering processes are stored in a map where the partial sums of their transition rates are used as key. The selected scattering process instance contains all essential information to update the statistics and the state variable.

holds, where the P_i are the partial sums of the scattering rates. The data structure for the selection method is given in Figure 7.3. As shown, the C++ standard template library containers are used with regard to minimizing the lookup time.

The actual state and the chosen scattering process are used to update the statistical quantities such as subband population, energy distribution, and current. Afterwards the state variable is set to its new value given by the scattering event. The MC loop is terminated when the given number of events is reached.

To account for the periodic structure of the device, the subbands of three stages are included. Whenever the electron scatters from the central to the left or the right stage it is reinjected into the corresponding state of the central stage, and the estimator for the electrical current is updated.

We identified the calculation of the polar-optical phonon scattering rate as one of the major contributions to the simulation run time. Therefore, we optimized the calculation of the scattering rate for this process by exchanging the order of the multiple integrations. An analytic integration over the final states is carried out first. The integration related to the matrix element is carried out last. The remaining integration is in momentum space and has the form

$$\Gamma_{mn}(\mathbf{k}_\parallel) = \frac{m^*}{\hbar^2}\frac{e^2\omega_{\mathrm{PO}}}{4\pi\varepsilon}\left(n_{\mathrm{PO}} + \frac{1}{2} \mp \frac{1}{2}\right)\int \frac{|\widehat{\rho}_{mn}(q_z)|^2}{\sqrt{(k_\parallel^2 + k_f^2 + q_z^2)^2 - 4k_\parallel^2 k_f^2}}\mathrm{d}q_z,$$

where $k_\mathrm{f}^2 = k_\parallel^2 + \frac{2m^*}{\hbar^2}(\mathcal{E}_m - \mathcal{E}_n \pm \hbar\omega_\mathrm{PO})$ has to be positive in order to satisfy energy conservation. This allows us to use a Fast Fourier Transform (FFT) to calculate the overlap integrals $\widehat{\rho}_{mn}(q_\mathrm{z}) = \mathcal{F}\{\rho_{mn}(z)\}$, where $\rho_{mn}(z) = \psi_m^*(z)\psi_n(z)$, which reduces the calculation time of the PO scattering rate by three to four orders of magnitude.

Currently, acoustic and optical deformation potential and polar optical electron-phonon scattering as well as alloy, intervalley, and interface roughness scattering are included. The object-oriented implementation allows for simple inclusion of additional physics for further investigation of QCL devices such as electron–electron and electron–photon interaction.

7.3 Results and Discussion

We used the implemented transport model to simulate the InGaAs/GaAsSb mid infrared (MIR) quantum cascade laser reported in [3]. The current density as a function of the electric field at 90 Kelvin is shown in Figure 7.4. The simulation result is in reasonable agreement with the experiment. The maximum in the current around the laser's designed optimum field strength can be attributed to a PO phonon resonance of the lower and ground laser level. The resonance causes a fast depletion of the lower laser level and aids the population inversion. The decrease in current above the threshold is due to increasing coherent tunneling to the continuum as well as the electron-photon interaction, which is not yet included in the model. At low fields the current is

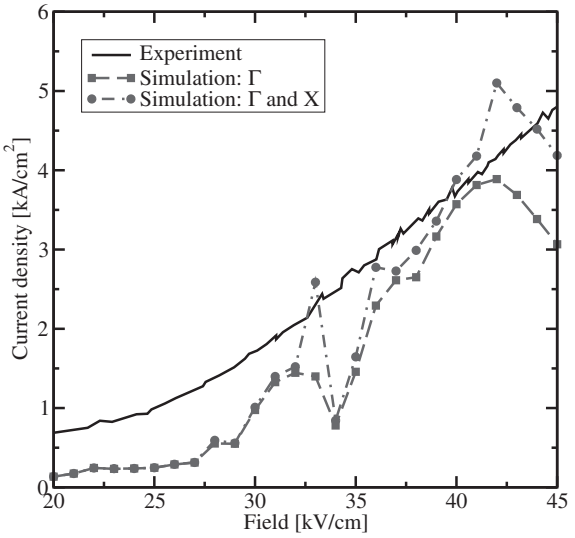

Figure 7.4. Current density vs. applied electric field of the MIR QCL. The simulation shows that the inclusion of the X valley has only a small influence on the characteristics around the laser threshold.

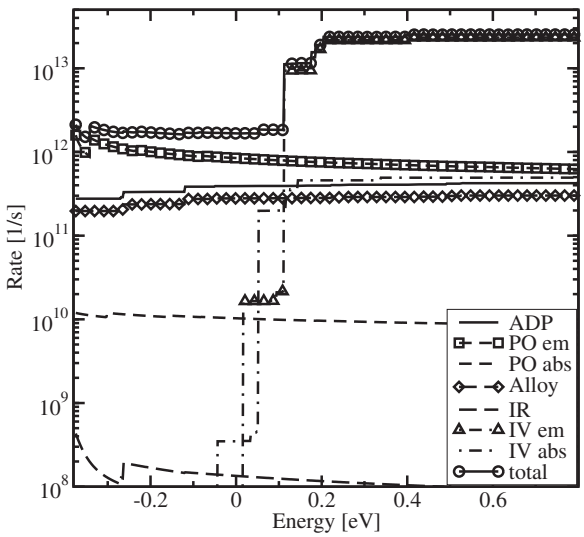

Figure 7.5. Calculated scattering rates with the lower laser level as initial subband. At energies near the subband minimum the polar optical emission is the dominant process. This ensures fast depopulation of the lower laser level.

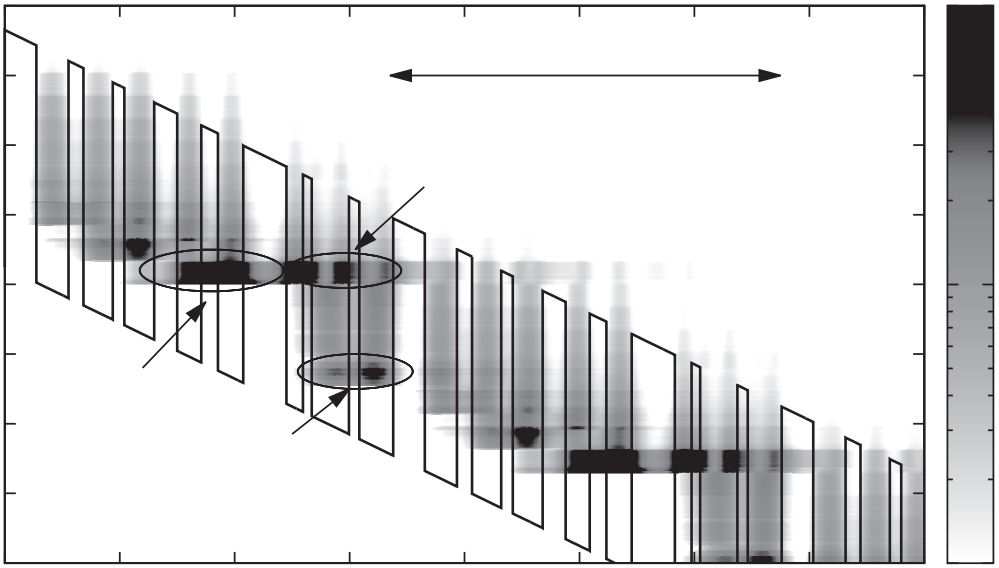

Figure 7.6. Conduction band edge and carrier density spectrum obtained by the Pauli master equation solver at an electric field strength of 40 kV/cm. The occupation of the upper laser state is clearly visible.

underestimated due to the dominant coherent transport through the barriers [13]. The characteristics show that transport in the X valley contributes only marginally to the total current near the laser threshold. This is also indicated by the scattering rates for the lower laser level (Figure 7.5), where PO emission is also shown to be dominant.

The calculation of a single operating point typically takes a few minutes, depending on number of valleys, subbands, and energy grid resolution. This is orders of magnitude faster than a full quantum treatment using nonequilibrium Green's functions, but still gives insight to microscopic quantities such as the carrier density spectrum shown in Figure 7.6.

7.4 Conclusion

We have presented a semiclassical transport model for quantum cascade lasers based on the Pauli master equation. We devised new numerical methods to reduce the computational demand and realized an efficient Monte Carlo simulator implemented in C++. The model was applied to a mid infrared QCL. It gives insight to macro- and microscopic quantities such as current-voltage characteristics, scattering rates, carrier density spectrum, subband population, and optical gain.

Acknowledgments. This work was supported by the Austrian Science Fund special research program IR-ON (F2509).

References

[1] J.-P. Berenger, A perfectly matched layer for the absorption of electromagnetic waves, *J. Comput. Phys.* **114** (1994), 185–200.

[2] R. Clerc, A. Spinelli, G. Ghibaudo, and G. Pananakakis, Theory of direct tunneling current in metal–oxide–semiconductor structures, *J. Appl. Phys.* **91** (2002), 1400–1409.

[3] H. Detz, M. Nobile, C. Deutsch, P. Klang, A. Andrews, W. Schrenk, K. Unterrainer, and G. Strasser, Improved InGaAs/GaAsSb quantum cascade laser active region designs, *Journal of Modern Optics* **58**(21) (2011), 2015–2020, available online at http://www.tandfonline.com/doi/abs/10.1080/09500340.2011.604734 (last accessed September 21, 2012).

[4] M. V. Fischetti, Master-equation approach to the study of electronic transport in small semiconductor devices, *Phys. Rev. B* **59** (1999), 4901–4917.

[5] C. Gmachl, F. Capasso, D. L. Sivco, and A.Y. Cho, Recent progress in quantum cascade lasers and applications, *Rep. Progr. Phys.* **64** (2001), 1533–1601.

[6] R. C. Iotti, E. Ciancio, and F. Rossi, Quantum transport theory for semiconductor nanostructures: A density-matrix formulation, *Phys. Rev. B* **72** (2005), 125347.

[7] R. C. Iotti and F. Rossi, Nature of Charge Transport in Quantum-Cascade Lasers, *Phys. Rev. Lett.* **87** (2001), 146603.

[8] C. Jirauschek, G. Scarpa, P. Lugli, M. S. Vitiello, and G. Scamarcio, Comparative analysis of resonant phonon THz quantum cascade lasers, *J. Appl. Phys.* **101** (2007), 086109.

[9] M. Karner, A. Gehring, S. Holzer, M. Pourfath, M. Wagner, W. Goes, M. Vasicek, O. Baumgartner, C. Kernstock, K. Schnass, G. Zeiler, T. Grasser, H. Kosina, and S. Selberherr, A Multi-Purpose Schrödinger-Poisson Solver for TCAD Applications, *J. Comput. Electron.* **6** (2007), 179–182.

[10] T. Kubis and P. Vogl, Self-consistent quantum transport theory: Applications and assessment of approximate models, *J. Comput. Electron.* **6** (2007), 183–186.

[11] S. C. Lee and A. Wacker, Quantum transport calculations for quantum cascade laser structures, *Physica E* **13** (2002), 858–861.

[12] R. B. Lehoucq, D. C. Sorensen, and C. Yang, *ARPACK Users' Guide: Solution of Large-Scale Eigenvalue Problems with Implicitly Restarted Arnoldi Methods*, Society for Industrial and Applied Mathematics, 1998.

[13] A. Mátyás, T. Kubis, P. Lugli, and C. Jirauschek, Comparison between semiclassical and full quantum transport analysis of THz quantum cascade lasers, *Physica E: Low-dimensional Systems and Nanostructures* **42** (2010), 2628–2631, 14th International Conference on Modulated Semiconductor Structures.

[14] G. Milovanovic and H. Kosina, A semiclassical transport model for quantum cascade lasers based on the Pauli master equation, *J. Comput. Electron.* **9** (2010), 211–217.

[15] S. Odermatt, M. Luisier, and B. Witzigmann, Bandstructure calculation using the $\mathbf{k}\cdot\mathbf{p}$ method for arbitrary potentials with open boundary conditions, *J. Appl. Phys.* **97** (2005), 046104.

[16] C. Sirtori, F. Capasso, J. Faist, and S. Scandolo, Nonparabolicity and a sum rule associated with bound-to-bound and bound-to-continuum intersubband transitions in quantum wells, *Phys. Rev. B* **50** (1994), 8663–8674.

Author information

Oskar Baumgartner, Institute for Microelectronics, Vienna University of Technology, Vienna, Austria.
Email: baumgartner@iue.tuwien.ac.at

Zlatan Stanojević, Institute for Microelectronics, Vienna University of Technology, Vienna, Austria.
Email: stanojevic@iue.tuwien.ac.at

Hans Kosina, Institute for Microelectronics, Vienna University of Technology, Vienna, Austria.
Email: kosina@iue.tuwien.ac.at